Yi-Jun Liu · Yen-Yu Chiu · Frank T.-C. Tsai · Su-Chin Chen

Analysis of landslide occurrence time via rainfall intensity and soil water index ternary diagram

Abstract This study introduces the soil water index (*SWI*) approach, the sum of water depths in the three-layer tank model, with rainfall data to understand landslide occurrence in Taiwan. A total of 236 historical instance data were compiled to investigate the characteristics of different types of landslides: debris flows (DF), shallow landslides (SL), and large-scale landslides (LL). The data shows that most DF occurred near the time of maximum rainfall intensity. However, several SL and LL events indicate that the occurrence of SL and LL has correlations with more than just rainfall intensity or rainfall amount. The *SWI* and the water depth in the tanks (from top to bottom: H_1, H_2, H_3) provide an intriguing approach to correlate soil moisture content at occurrence time with the landslide types. DF events show the highest H_1/SWI value, which indicates the correlation with water content in the surficial soil. LL events after rainfall have the highest H_3/SWI ratio, indicating that prolonged rainfall events cause rainwater to infiltrate a deeper soil layer and trigger these LL. We developed a ternary diagram of the water depth-to-*SWI* ratios to show characteristics of the three landslide types. This study found that the H_2/SWI value is typically in the range of 0.2–0.4. In this range, the landslide type gradually shifts from DF to SL, and then to LL, along the H_3/SWI axis. Therefore, the ternary diagram can explain landslide type changes with the water depth-to-*SWI* ratios and better understand landslide occurrence.

Keywords Rainfall · Debris flow · Landslide · Occurrence time · Tank model · Soil water index

Introduction

Rainfall-induced landslides are one of the most common natural hazards globally and often result in a catastrophic loss of life and substantial property damage. After rainfall infiltrates the soil, the percolation process will increase soil moisture content on hills and elevate the water table (Bogaard and Greco 2018). Increased pore water pressure or increased soil weight may then cause gravitational shear stress within a hill to exceed resisting shear strength, induce slope failure, and lead to landslides of various sizes. Based on the magnitude of slope failure, landslides can be classified into shallow landslides (SL) and large-scale landslides (LL). SL typically occur in unsaturated soil layers or at the boundary of weathered surface soil and bedrock. Consequently, most SL have a shallower sliding surface and a smaller size. In contrast, LL are typically characterized by gravity deformation with a deeper sliding surface (Hutchinson 1988; Dille et al. 2019) and a larger size. Moreover, it takes a longer time to trigger LL. Various LL are defined based on the size in the literature (Tamura et al. 2008; Safran et al. 2011; Tfwala et al. 2020), such as landslide area > 10 ha, landslide depth > 10 m, or landslide mass > 100,000 m³. However, because landslide depth is not an adequate basis for landslide classification, this study adopts the definition of SL as a landslide area < 10 ha and LL as a landslide area ≥ 10 ha, and depth ≥ 2 m proposed by the *Soil and Water Conservation Bureau* of Taiwan, and some studies have adopted the definition (Wu et al. 2016; Tfwala et al. 2020). It was impossible to exactly investigate landslides of occurrence time in the past. However, the advance of technology and the development of more monitoring methods have made it possible to pinpoint when landslides occur accurately. Due to the increased frequency and intensity of extreme rainfall events in recent years (Gariano and Guzzetti 2016), the frequency and magnitude of landslides have also increased (Obeysekera and Salas 2016; Sangelantoni and Gioia 2018), and consequently, there have been more LL. Due to Taiwan's geographical location, topography, and geological conditions, landslides and debris flow (DF) events commonly occur following typhoons and torrential rains. Therefore, this study investigates landslides throughout Taiwan, including the DF events that often happen in Taiwan's mountainous areas.

Although physical mechanisms or statistical models can analyze rainfall-induced landslides, physical models typically involve many parameters, such as rock composition, weak planes, cohesion, and friction angle. These parameters could not always be available in all landslide investigations. The use of physical models in the analysis under several assumptions or neglecting various factors may render the modeling results less meaningful. The most often seen statistical analysis method is the empirical formula method, which employs rainfall conditions, including rainfall intensity, rainfall duration, accumulated rainfall, and antecedent rainfall, to determine relevant rainfall warning thresholds. Those popular empirical formulas involve the rainfall intensity-rainfall duration (*I-D*) relationship (Caine 1980; Larsen and Simon 1993; Guzzetti et al. 2007; Brunetti et al. 2010). However, Saito et al. (2010) indicated that the *I-D* method could only express average rainfall during an event and does not necessarily account for the effect of antecedent rainfall and sporadic high-intensity rainfall events. Rosi et al. (2012) emphasized that the starting point of rainfall events can influence the calculation of a rainfall threshold. Furthermore, the *I-D* method may not determine the time at which a landslide occurs when rainfall is about to stop. Bogaard and Greco (2018) analyzed landslide and DF thresholds from the perspective of hydrometeorology. They suggested that soil water index (*SWI*) can serve as a critical variable in determining the thresholds of rainfall-induced landslides.

The *SWI* is the sum of water depths in the three-layer tank model with defined parameter values (Sugawara et al. 1974; Ishihara and Kobatake 1979). In this model, the three tanks from top to bottom represent the surface, middle, and deep layers of a soil column. The tank model simulates infiltration and seepage of rainwater in the soil and can correlate rainfall infiltration and soil moisture content with landslide occurrence given different rainfall conditions. Many studies have shown that *SWI* can indeed be applied to landslide analysis and used in warning systems. Suzuki et al. (1979) used the tank model to analyze DF in Japan's Mount Rokko area. Results indicated that DF events tend to occur during the peak water depths in the first and the second tanks. Michiue (1985) used the tank model to analyze landslides in the Japanese city of Kure and found that the landslides occur when $SWI > 70$ mm. Osanai et al. (2010) described how the Japan Meteorological Agency established a landslide warning system with 5-km grid spacing based on the *SWI*. In an analysis of SL and DF events in Taiwan, Chen et al. (2013) found that the occurrence of SL and DF correlates highly with the depths of the first and the second tanks. Chen et al. (2017) employed *SWI* to analyze rainfall-induced mass wasting in Taiwan and found that the increase in the *SWI* in rainfall events of different types has a close relationship with the occurrence of landslides and recommended that *SWI* be applied to landslide forecasting. Lin et al. (2020) used the tank model to analyze LL, established a relationship between *SWI* and rainfall duration, and proposed that a better correlation exists between the occurrence of LL and the water depth of the third tank than that of the first tank, but did not clearly indicate the relationship between the time of occurrence and the different types of landslides.

An overall comparative analysis of DF, SL, and LL characteristics is rarely seen in the literature and is the scope of the study. We first collected cases of different landslides, examined the rainfall conditions at times DF, SL, and LL occurred, then analyzed *SWI* and the water depth in each tank to explore the DF, SL, and LL characteristics at occurrences. We inferred the tendency of water distribution in the soil column with respect to the three types of landslides. Lastly, we used the ratio of water depth of the three tanks to establish a *SWI* ternary diagram.

Materials and methods

Study area

Taiwan (Fig. 1) is located at the plate boundary where the Eurasian Plate collides with the Philippine Sea Plate and has frequent earthquakes. With a total area of 36,000 km², northern Taiwan is affected by mid-latitude frontal systems and cold air masses, while southern Taiwan is influenced by tropical systems, along with frequent typhoons and tropical depressions. Taiwan as a whole has a subtropical monsoon climate, and rainfall is plentiful. The average annual rainfall is approximately 2500 mm, and 60–80% of the rain falls during the rainy season (May–October). In addition, Taiwan's geographical location caused her to encounter 3 to 4 typhoons each year in general. Mountains cover almost two-thirds of Taiwan, and several mountain ranges have north–south trending structures. In particular, the Central Mountain Range runs north–south throughout nearly the entire island, dividing her into western and eastern halves. The western half consists mainly of lowland plains. Areas with an elevation > 1000 m account for 32% of the island, as seen in Fig. 1. Furthermore, significant variation exists in slopes; land with a hill slope > 10° accounts for 65% of Taiwan's land area. In summary, Taiwan's topographical characteristics and young and fragile geology, along with typhoons and torrential rains in the rainy season, render landslides frequently.

Landslide data

This study obtained data on three different landslides: SL, DF, and LL, from the Soil and Water Conservation Bureau. Human or earthquake-induced events have been ruled out firstly. The dataset covers 50 DF and 92 SL events from 2010 to 2019. This dataset consists of in situ surveys, landslide size, length, width, occurrence time, and location but does not provide the DF area in detail. Concerning the LL data, the Soil and Water Conservation Bureau used landslide earth movement signals recorded by the *Broadband Array in Taiwan for Seismology* to obtain the exact times and locations of landslides between 2001 and 2016 and provided data on 95 LL events during this period. The landslide seismic signals have shown the effectiveness of recording the exact times and locations of surface shaking generated by landslides (Dammeier et al. 2011; Manconi et al. 2016; Kuo et al. 2018). Figure 1 shows the locations and sizes of collected SL, DF, and LL. While most DF and SL occurred at elevations below 500 m, most LL occurred between 1000 and 1500 m. DF were generally in areas with slopes < 10°, SL essentially occurred in areas with slopes between 20 and 30°, and LL mainly occurred on slopes above 30° but below 40°. Fewer instances of SL and LL were at slopes greater than 40°. Seventy-one percent of SL sizes had an area < 2 ha, and 62% of LL had an area between 10 and 20 ha. The rainfall condition is one of the focuses of this study, by which we distinguished SL and LL. Eleven percent of SL instances occurred during a rainfall event, while 27% of the LL occurred after the rain stopped.

Rainfall data

We first used the *ArcGIS* "Generate Near Table" geoprocessing tool to find the nearest rainfall station to each landslide site and then confirmed each rainfall station in conjunction with manual identification. Rainfall data of 7 days (168 h) before the beginning of an effective rainfall event serves as antecedent rainfall. In the study, the start time of an effective rainfall event is determined
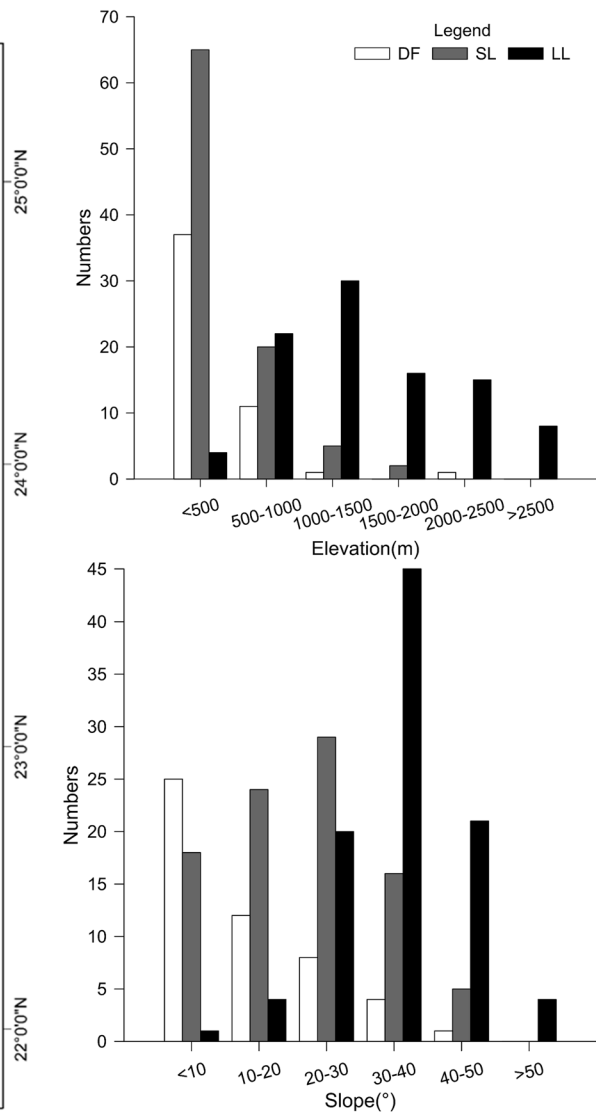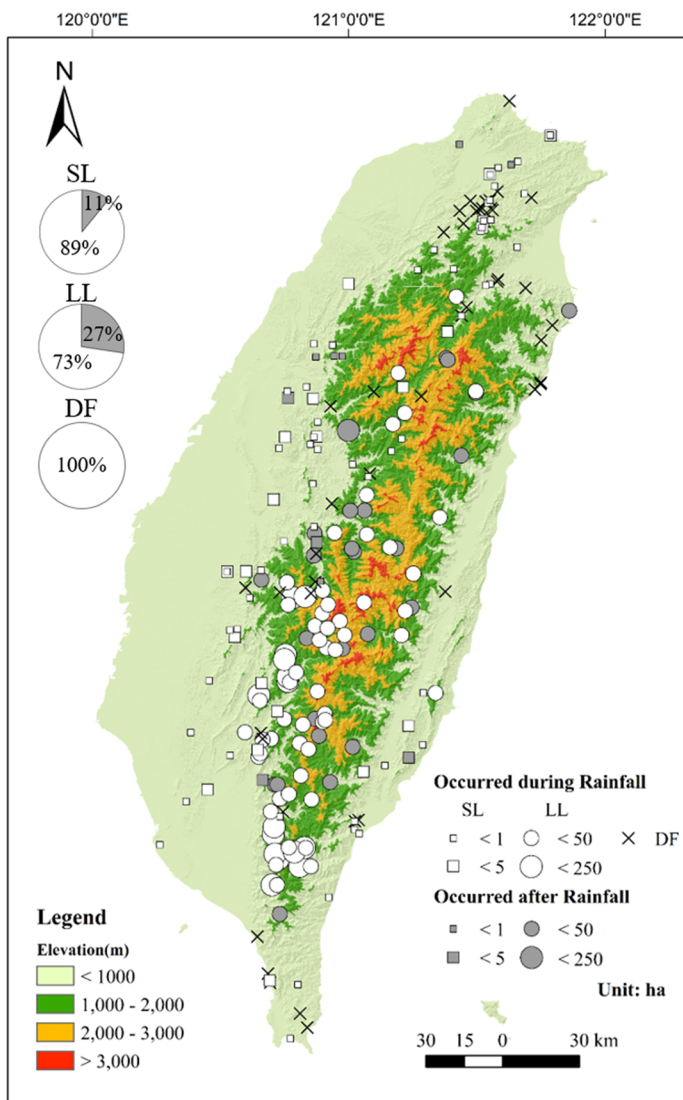
Fig. 1 Location and size of landslides with respect to elevations and slopes

when rainfall intensity is greater than or equal to 4 mm/h, and the time after rainfall intensity less than 4 mm/h for 6 continuous hours is taken as the end (consistent with Jan and Lee 2004; Lee 2006; Kuo et al. 2018). The period between the start and end points of each rainfall event is defined as the rainfall duration (T_R). The occurrence time (T_o) of a landslide is the time from the start of the rainfall event to the time a landslide occurs, as shown in Fig. 2. Landslides may occur during rainfall or after rainfall. Accumulated rainfall (R_A) is the sum of the total rainfall in the event and the antecedent rainfall. H_1, H_2, and H_3 are the water depth of the first, second, and third tanks, respectively.

Soil water index

Nash (1957) developed the rainfall-runoff conceptual model of a watershed as *n* series reservoirs, named as a tank model. Sugawara (1961) advanced the tank model concept to simulate water depths in a soil column as a series of tanks for the landslides disaster (Fig. 3). The tank model is based on the water balance principle with defined model parameters shown in Table 1. The *SWI* represents the soil moisture content which is the sum of water depths in the three layers of the tank model (Okada et al. 2001). Past research has shown that *SWI* can
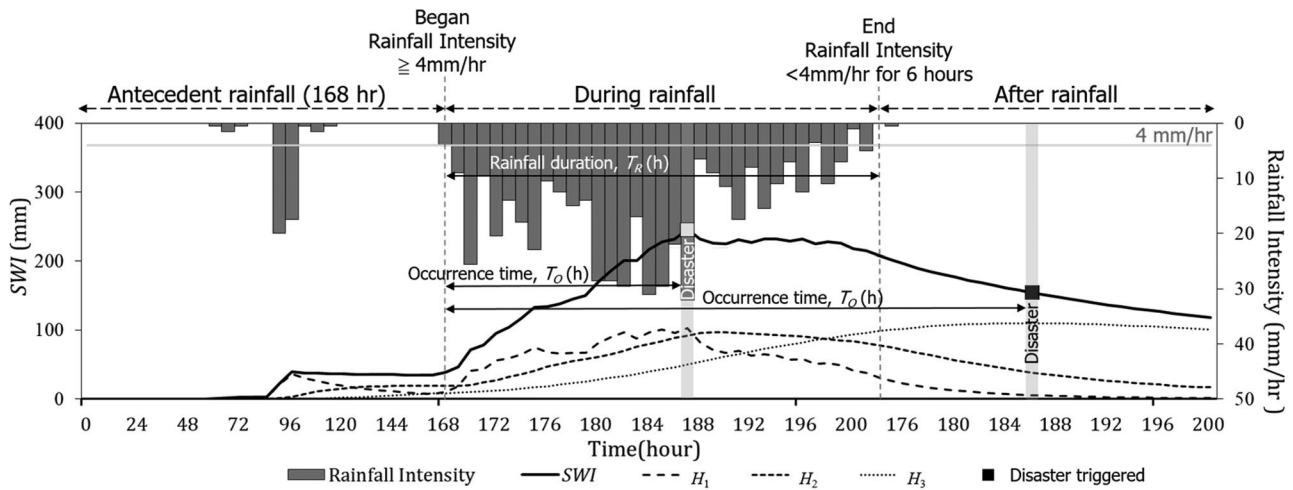
Fig. 2 Illustration of a rainfall event and associated rainfall intensity, *SWI* hydrograph (the sum of water depths in the three tanks), during-rainfall landslide occurrence time, and after-rainfall landslide occur-rence time. H_1, H_2, and H_3 represent the tank water depth from top to bottom

analyze and forecast the times at which various types of land-slides may occur (Suzuki et al. 1979; Michiue 1985; Osanai et al. 2010; Chen et al. 2013, 2017; Lin et al. 2020), and the water depth in each tank was correlated to different types of landslides. For instance, the water depth in the first and the second tanks may forecast DF and SL, and the water depth in the third tank may forecast LL. The Japanese government used *SWI* to establish a landslide early warning system starting in 2006. This system employs 60-min accumulated rainfall and *SWI* to establish land-slide early warning standards in 5-km grid cells (Osanai et al. 2010). If the water depths in the three-layer tanks increase, the probability of a landslide to trigger will rise. The method of calculating the *SWI* is explained as follows.

Consider that $H_k(t + \Delta t)$ is the water depth in tank k at time $(t + \Delta t)$ and $k = 1$, 2, and 3 are the tank indices from top to bottom. *SWI* is the sum of water depth in the three tanks (Okada et al. 2001):

$$\text{SWI}(t + \Delta t) = \sum_{k=1}^{3} H_k(t + \Delta t) \tag{1}$$

According to the water balance equation, water level $H_k(t + \Delta t)$ in each tank is computed for every hour ($\Delta t = 1$h) as follows:

$$H_k(t + \Delta t) = \begin{cases} H_k(t) - \left[\sum_i O_{ki}(t) + F_k(t)\right]\Delta t + R(t)\Delta t, & (k = 1) \\ H_k(t) - \left[O_k(t) + F_k(t) - F_{k-1}(t)\right]\Delta t & (k \geq 2) \end{cases} \tag{2}$$
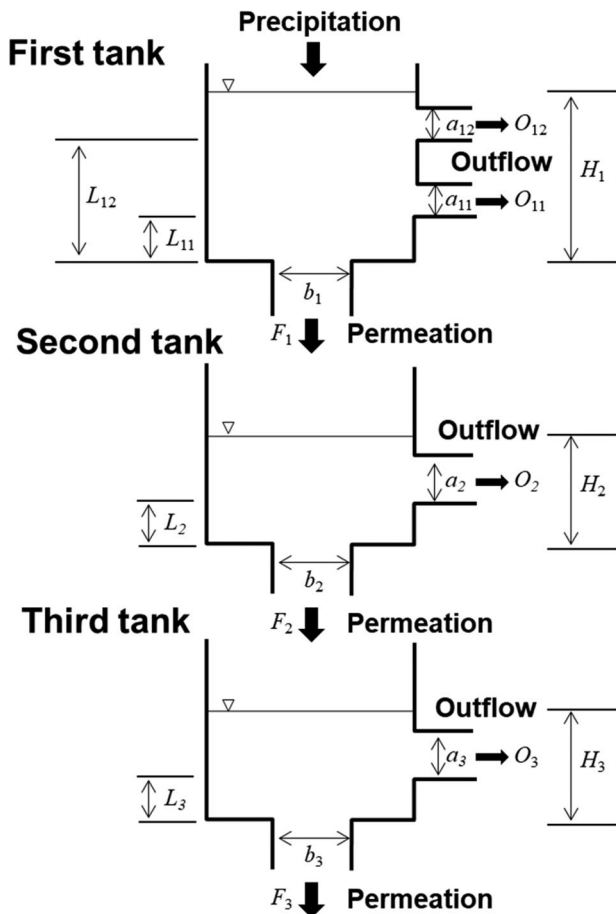
Table 1 Parameters for each tank of *SWI* (Ishihara and Kobatake 1979)

Fig. 3 Conceptual drawing of the tank model (Okada et al. 2001)

Tank	Outflow height (mm)		Outflow coefficient (h⁻¹)		Coefficient of permeability (h⁻¹)
First	$L_{11} = 15$	$L_{12} = 60$	$a_{11} = 0.1$	$a_{12} = 0.15$	$b_1 = 0.12$
Second	$L_2 = 15$		$a_2 = 0.05$		$b_2 = 0.05$
Third	$L_3 = 15$		$a_3 = 0.01$		$b_3 = 0.01$

where O_{ki} and O_k are the side leakage of the tanks. The top tank has two side outlets ($i = 1, 2$). F_k is the water that permeates down to the ($k + 1$) tank below. $R(t)\Delta t$ represents the rainfall amount in the time interval Δt. The outflow and the permeation are calculated as follows:

$$O_{ki}(t) = \begin{cases} 0, & (k = 1 \ and \ H_k(t) \leq L_{ki}) \\ 0, & (k \geq 2 \ and \ H_k(t) \leq L_k) \\ \alpha_{ki}[H_k(t) - L_{ki}], & (k = 1 \ and \ H_k(t) \leq L_{ki}) \\ \alpha_k[H_k(t) - L_k], & (k \ and \ H_k(t) \leq L_k) \end{cases} \quad (3)$$

$$F_k(t) = b_k H_k(t) \quad (4)$$

where L_{ki} and L_k are the height of the leakage, and a_{ki} and a_k are the outflow coefficients. F_k is the vertical permeation from the kth tank, and b_k is the coefficient of permeability of the kth tank.

Results and discussion

Correlation of rainfall characteristics with landslide occurrences

The rainfall intensities and accumulated rainfalls with landslide occurrence time of all instances are shown in Figs. 4 and 5. The results show a strong correlation between the occurrence of DF and rainfall intensity, and DF events are most likely to occur from the time of maximum rainfall intensity to 3 h afterward. The DF tend to occur during rainfall, 90% of DF events (45 times) occur when rainfall intensity is greater than 10 mm/h, and the median occurrence time is 21 h. The statistical results also reveal that 58% of DF events (21 times) occurred at the maximum rainfall intensities, and 18% of DF events (9 times) occurred within 3 h after the maximum rainfall intensities. Figure 6 shows two DF incidents; Fig. 6a shows an incident occurring at peak rainfall; Fig. 6b shows the occurrence time within 3 h after peak rainfall. Eleven percent of SL (10 times) and 27% of LL (26 times) occurred after rainfall, and the two types of the landslide had a relatively wide range of rainfall intensities at their time of occurrence. This result indicates that rainfall intensity and maximum rainfall intensity are not the influential critical factors to the events of SL and LL.

The median SL occurrence time was 19 h, and the median LL occurrence time was 41 h. DF and SL both had shorter occurrence times than LL, indicating that LL require a relatively longer infiltration time. Most landslide sizes > 50 ha had an occurrence time of > 40 h. However, the correlation between landslide size and time of occurrence was weak. In addition, there was no significant correlation between the size of SL and LL events and rainfall intensity.

Fig. 4 Scatter plot of rainfall intensity versus landslide occurrence time under different sizes of the landslide area
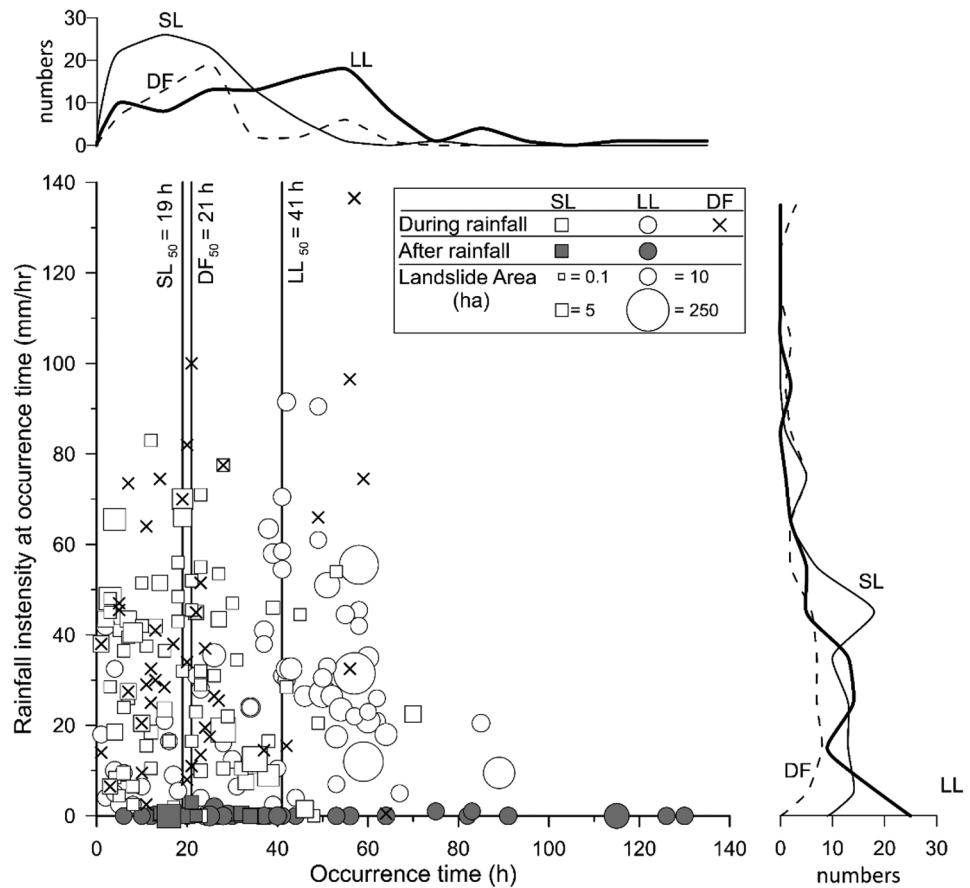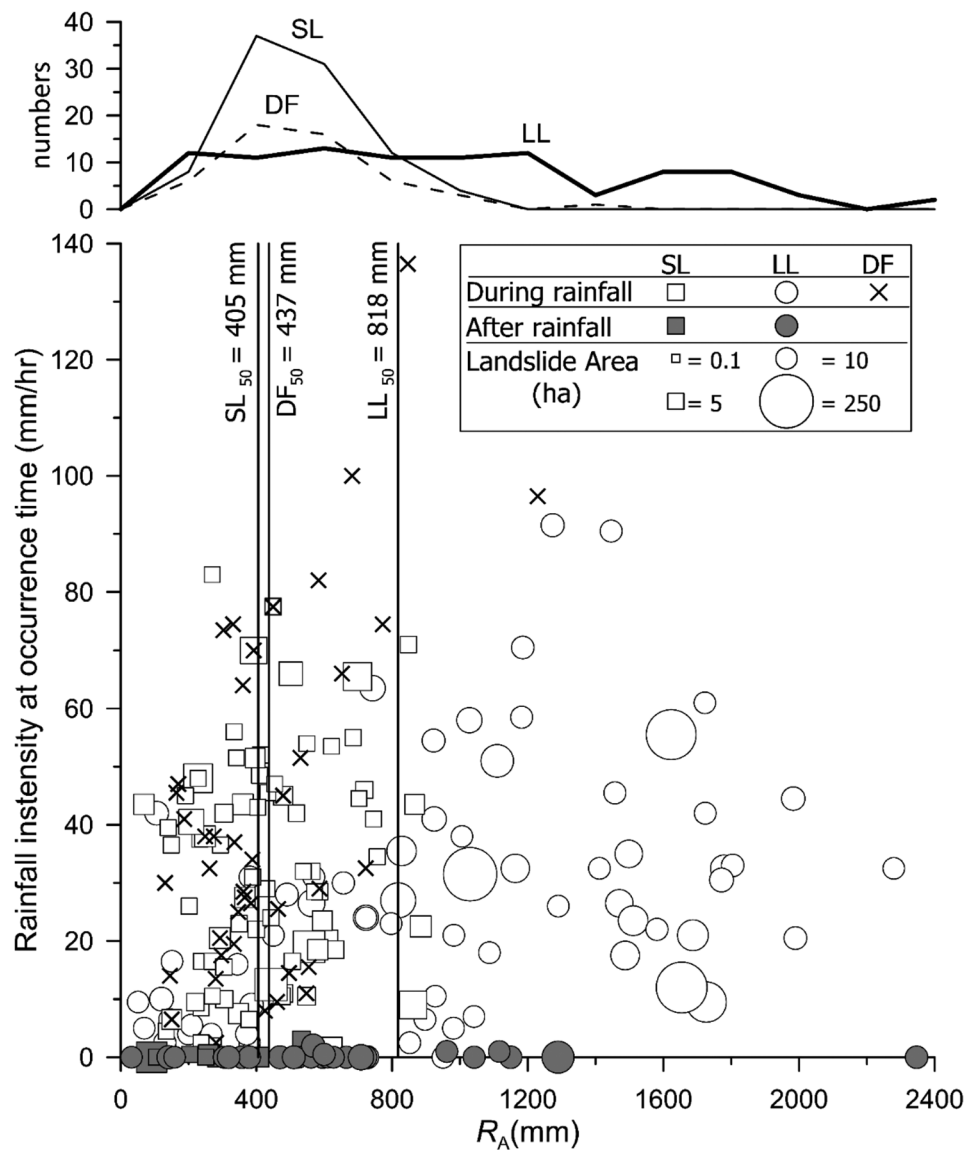
Fig. 5 Scatter plot of accumulated rainfall versus the rainfall intensity at occurrence time under different sizes of the landslide area

From the accumulated rainfall analysis (Fig. 5), most DF events occurred when accumulated rainfall was in a range of 175–800 mm, with the median (DF_{50}) of 437 mm. Most SL events occurred when the accumulated rainfall was between 200 and 750 mm, with the median (SL_{50}) of 405 mm. Most LL events occurred during a wide range of accumulated rainfall values, with the median (LL_{50}) of 818 mm. The accumulated rainfall depths of LL events were significantly higher than those of DF and SL. All landslides with a size greater than 100 ha occurred when accumulated rainfall exceeded 800 mm. This indicates that high accumulated rainfalls may trigger LL.

Relationship between maximum rainfall intensity and landslide occurrence time

In order to shed light on the relationship between rainfall intensity and landslide occurrence time, this study discusses landslide occurrence time before, during, and after the maximum rainfall intensity. We normalized rainfall intensity (I) by the maximum rainfall intensity (I_{max}) and normalized landslide occurrence time (T_o) by the rainfall duration (T_R) and show their correlation in Fig. 7.

Figure 7a reveals that no DF instance occurred after the rain stopped, in contrast to SL and LL. The T_o/T_R ratios of the SL and LL events were broadly distributed, compared to DF events as shown in Fig. 7b, c. Most instances of SL and LL occurring after rainfall had a $T_o/T_R < 3.0$, with the 10 cases of LL that had a T_o/T_R ratio of 1.0–1.2. This indicates that instances of LL occurring after rainfall generally tend to occur not long after the rain stops.

The majority of landslides that occurred after I_{max} was LL (77.9%), followed by SL (53.3%) and DF (32%). The 43 instances of LL occurring after I_{max} had a T_o/T_R ratio in the range of 0.4–1.0, while the 29 cases of SL occurring after I_{max} had a T_o/T_R ratio in the range of 0.5–1.0. The lack of SL and LL instances in a low T_o/T_R ratio indicates that both SL and LL tend to occur
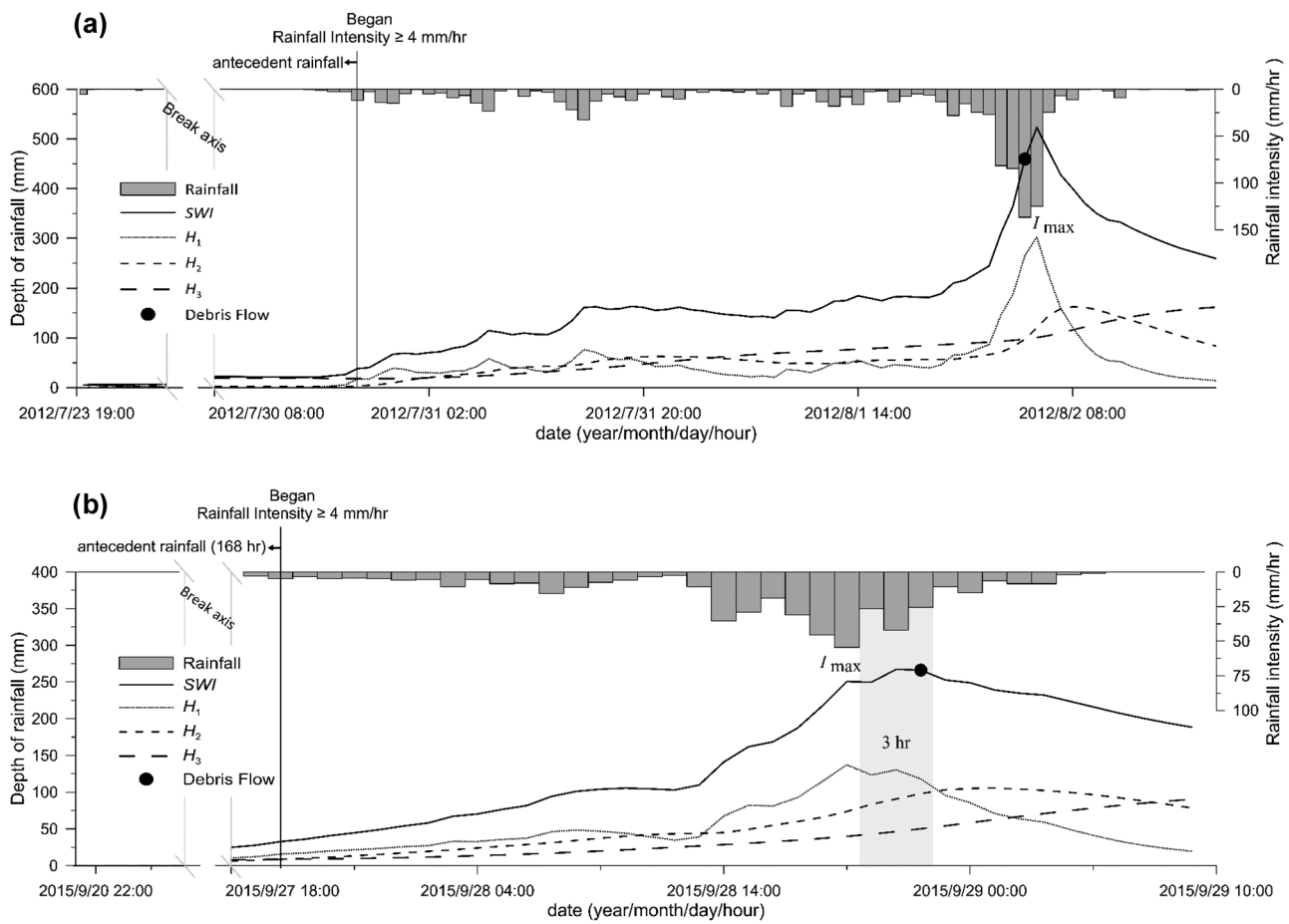
Fig. 6 Events of DF occurrence near the maximum rainfall intensity. **a** A DF event occurred at peak rainfall, and **b** a DF event occurred within 3 h after peak rainfall

when rainfall has accumulated for a certain period, and rainwater infiltration and soil moisture content have risen to a certain degree.

However, instances of SL and LL occurring after I_{max} or after rainfall indicate that the use of rainfall intensity and accumulated rainfall alone cannot fully explain the initiation of these landslides. This implies that soil moisture may considerably influence these landslide occurrences. Therefore, we employed SWI in the subsequent analysis.

Relationship between landslides and rainfall intensity and SWI

The SWI and occurrence time have a stronger positive correlation for the clusters of landslide events during the rainfall than those after the rainfall (Fig. 8). The SWI of DF events is primarily in the range of 150–400 mm, with a median of 236 mm; the SWI of SL events is mainly in the range of 100–300 mm, with a median of 206 mm; and the SWI of LL events displays no significant distribution trend, with a median of 271 mm (Fig. 8). The SWI of LL is typically higher than that of DF and SL, and landslides with a size > 100 ha tend to occur when $SWI > 300$ mm.

Figure 9 shows the routes of the SWI and the corresponding accumulated rainfall (R_A) of landslide instances. The progress is classified into two stages: the rising and falling stages. When rainfall begins, SWI and accumulated rainfall increase in the rising stage until they reach peak values. Afterward, as the rainfall intensity decreases, a falling stage begins. During this stage, while SWI falls continuously, accumulated rainfall will increase slightly or remain unchanged. Our results indicate that most DF events occur during the rising stage, consistent with actual DF occurrence conditions, including heavy rainfall. Many instances of DF occurred when the ratio of SWI to accumulated rainfall was in the range of 0.5–0.9. Linear regression shows that
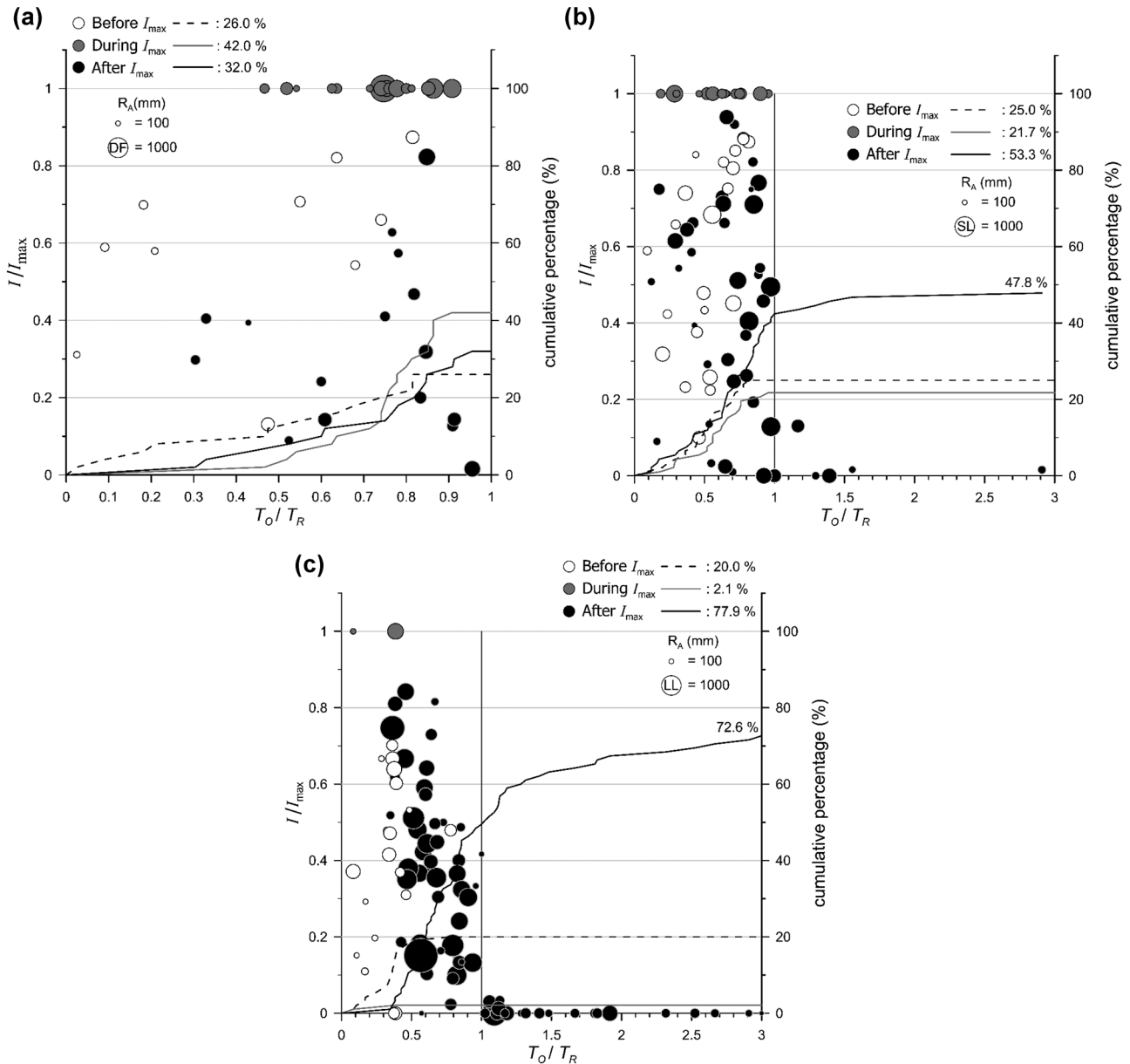
Fig. 7 Scatter plots of the normalized occurrence time (T_0/T_R) versus the normalized rainfall intensity (I/I_{max}) (**a** DF, **b** SL, and **c** LL)

the *SWI* value is 0.52 times of the accumulated rainfall. Most instances of SL occurring in a rainfall event took place during the rising stage, and only a small number of cases, as well as those SL events occurring after rainfall, occurred during the depletion stage. Most SL events occurred when the ratio of *SWI* to accumulated rainfall of these events was within 0.4–0.9. The *SWI* at SL occurrence during rainfall is 0.46 times of the accumulated rainfall and is 0.31 times of the accumulated rainfall after rainfall.

Unlike DF and SL events, LL events mainly occur during the falling stage, regardless of the landslide occurrence time. During the falling stage, the accumulated rainfall increases slowly or remains unchanged. Consequently, the ratio of *SWI* to accumulated rainfall instances of LL has a relatively broad distribution, but it is usually less than 0.5. In addition, when LL events occur after rainfall because rainfall has already stopped, the *SWI* will decrease gradually with time. This will result in significant discrepancies in the ratio of *SWI* to accumulated rainfall for LL

Fig. 8 Distribution of landslide events with the occurrence time and the *SWI*
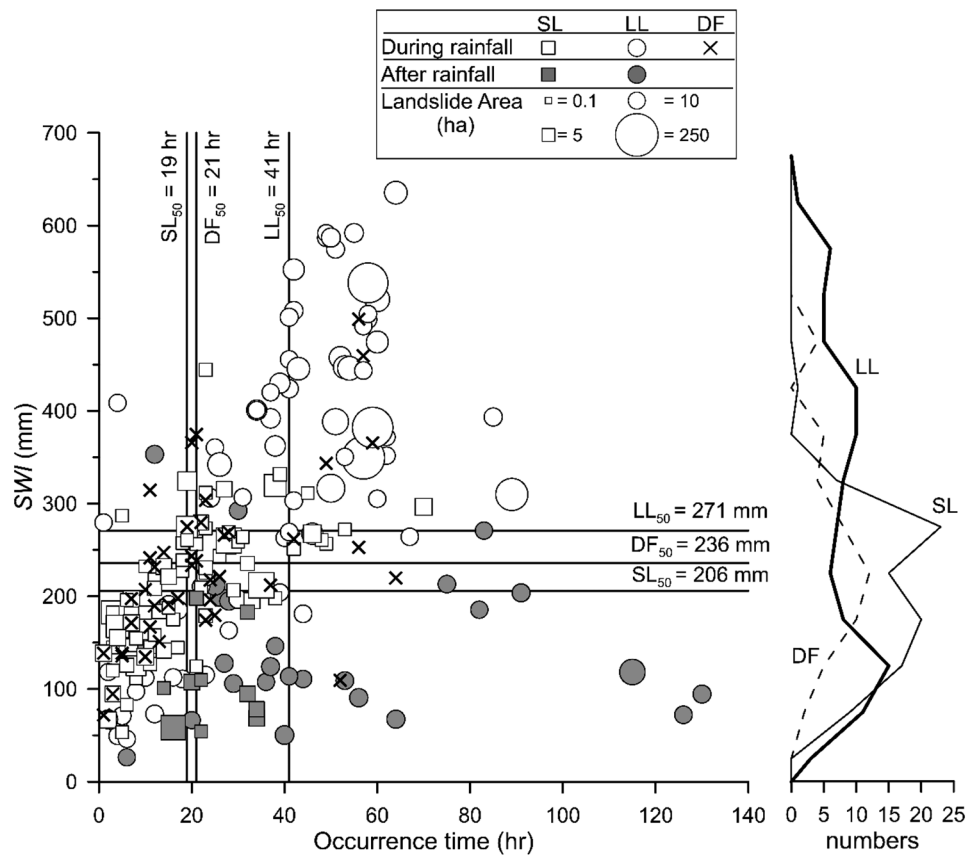
events. The *SWI* of LL events occurring during rainfall is 0.30 times of the accumulated rainfall, and the *SWI* value of LL events occurring after rainfall is 0.19 times of the accumulated rainfall. Compared with SL and DF, LL may take place over a more extended period, accounting for a small ratio of *SWI* to R_A. In other words, as this ratio becomes larger, rainfall has a growing influence on the *SWI*. And conversely, when this ratio becomes smaller, the landslides are less influenced by rainfall but more influenced by the *SWI*, such as LL.

Relationship between landslide occurrence time and tank water depths

In principle, water depths in the three tanks reach their respective peaks in chronological order from the top tank to the bottom tank. This study, therefore, establishes four commonly occurring water depth situations when a landslide occurs (Fig. 10). If a landslide occurs while the water depths in all three tanks increase, it is classified as type 1. This situation indicates that the landslide occurred during the early part of a rainfall event. If a landslide occurs while the water depth in the first tank decreases, but the water depths in the second and the third

tanks continue to increase, it is classified as type 2. This situation indicates that rainfall has already continued for a certain period prior to the landslide, and a transient decrease in rainfall has caused the water depth in the first tank to stop rising. If a landslide occurs while the water depths in the first and the second tanks decrease and only the third tank has increasing water depth, it is classified as type 3. This situation indicates that rainfall is about to stop, and rainwater has reached the deeper soil layer. As a consequence, the water depth in the third tank continues to rise. If a landslide occurs while the water depths in all three tanks decrease continuously, it is classified as type 4. This situation may occur under two circumstances: First, a landslide occurs after rainfall when infiltrated water has already gradually dispersed, and second, due to the influence of antecedent rainfall, a landslide is triggered at the beginning of the next rainfall.

Figure 11 shows the statistics of DF, SL, and LL in these four types. In comparison, SL events have a relatively average distribution among these four types: 70% (58 cases of SL instances that occur during rainfall concentrate in type 1 and type 2, 80% of SL occurring after rainfall belonging to type 3, 81% of LL occurring during rainfall concentrate in type 2 and type 3 and all LL occurring after rainfall in type 3 and type 4, and 62% of
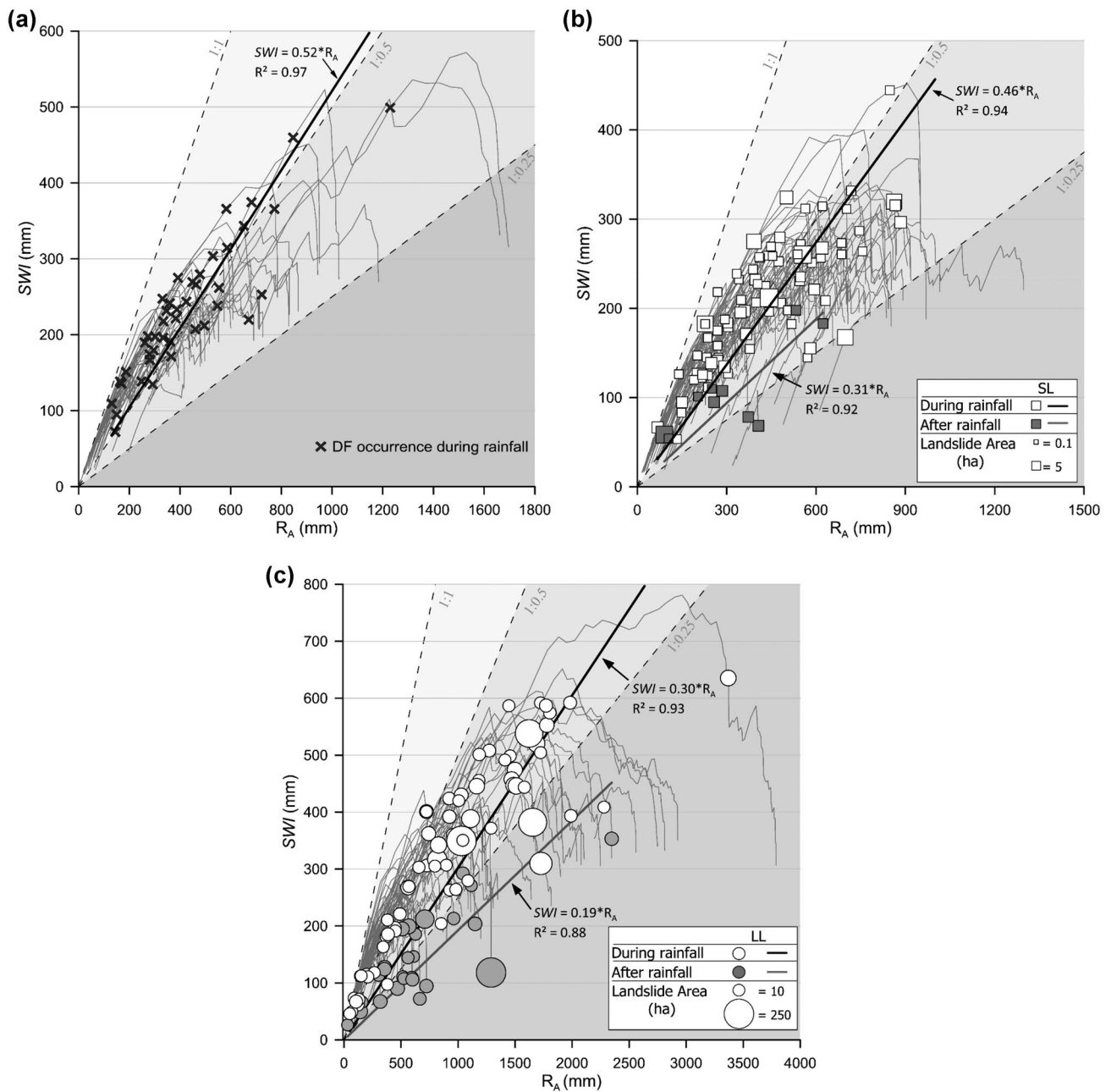
Fig. 9 Distribution of cumulative rainfall and the *SWI* routes for **a** DF, **b** SL, and **c** LL

DF events concentrating in type 1. This is consistent with Suzuki et al. (1979), suggesting that the time at which DF occur is close to the time of peak water depth in the first and the second tanks. A comparison reveals that DF events tend to occur during the early period of rainfall, so water depth in all three tanks continues to rise. In comparison, SL events show an average distribution in the four types indicating an elusive characteristic. Most LL events occur when the water depths in the second and the third tanks are near their peak. This infers a lack of connection between LL and water content in the surface layer. These inferences can be further investigated by analyzing the ratios of water depths in the three layers to the *SWI* in the next section.
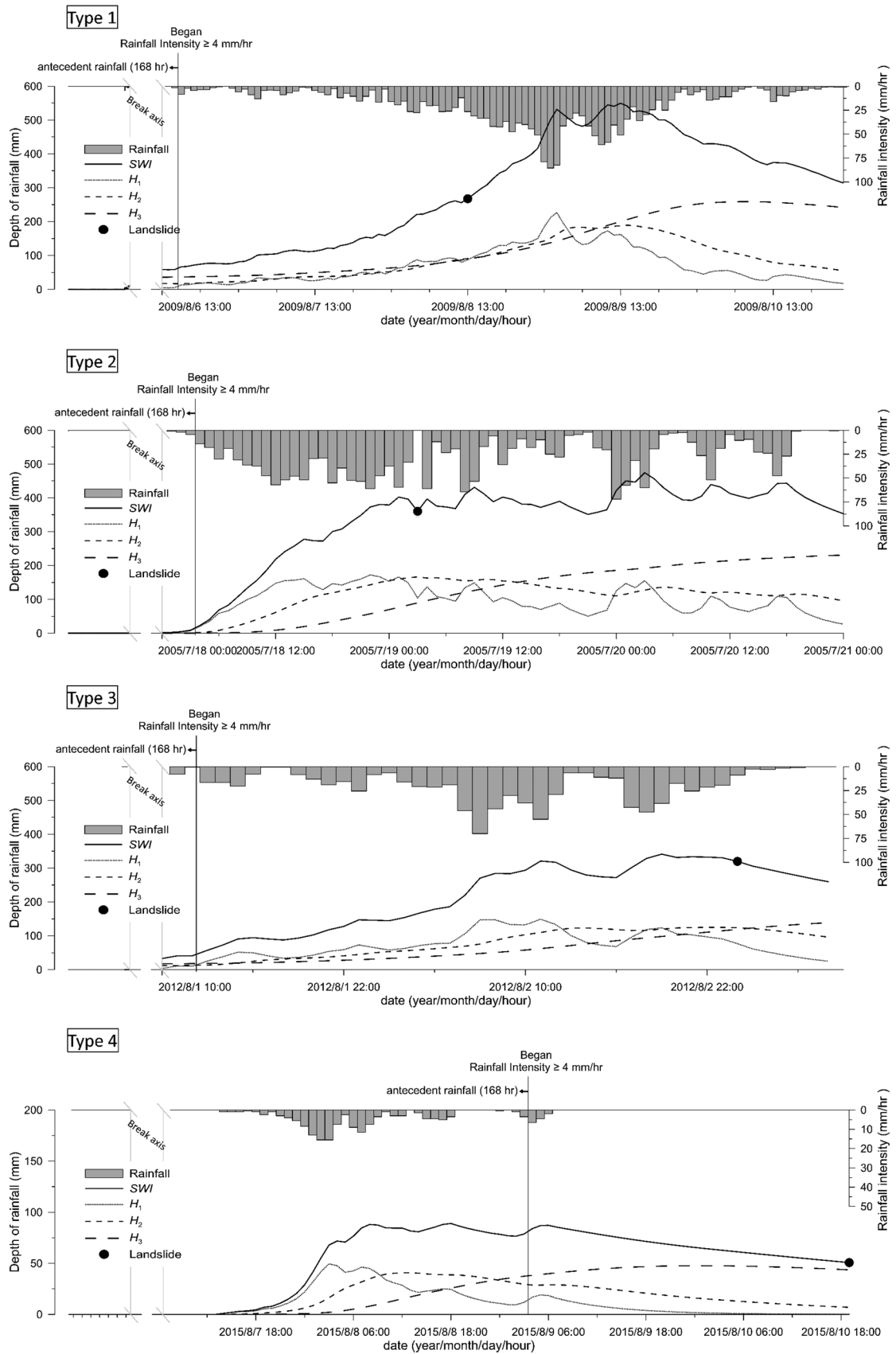
Fig. 10 Examples of the 4 types defined based on water levels and landslide occurrence time
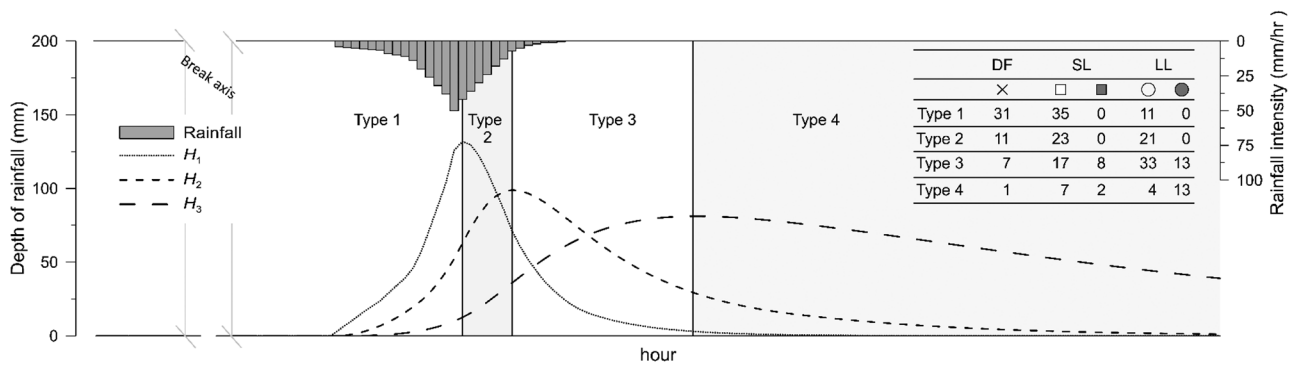
Fig. 11 Statistic distribution of the instances for the 4 types

The ratio of water depth to SWI in each tank at landslide occurrence time

The ratio of each tank water depth to SWI at landslide occurrence time can infer the state of seepage movement in the soil and the characteristics of landslides. A ternary diagram with the water depth fractions (the ratio of the water depth of each tank to SWI) on the three axes can express the water content distribution in the soil column when landslides occur. Figure 12a shows the ternary clustering by the classification in Fig. 10, according to the variation (increasing or decreasing) of water depth in each tank. The distribution zones of the four types are ordered; cases belonging to type 1 mainly appear in the left down part of the diagram where the fractions of H_1 are more significant than the other fractions, as a result of the events in type 1 occurring early in the rainfall events and also expressing an unsaturated condition in the soil layer. When the soil is gradually saturated in the rain, the condition of type 2 and type 3 is reached successively. The progress accompanies the decrease in the fraction of H_1 and the increase of H_3. Therefore, the occurrences of landslides in these cases are attributed to the movement of water in the soil layer, while type 4 occurs when the water depths are all decreased and present the highest H_3 fraction, inferring that the other reasons, like the raised groundwater table, caused the occurrence of landslide. Figure 12b clusters the data according to the landslide type as shown in the legend. The clusters in Fig. 12b have broader dispersed distributions than those in Fig. 12a. Nevertheless, DF events show higher fractions of the first tank that are consistent with the understanding that DF events occur when rainfall is plentiful, and water has reached a considerable soil depth meanwhile. In contrast, LL events occur when the first tank fraction is small, which indicates that water in the surface soil has gradually dispersed and infiltrated deeper layers. Furthermore, SL and LL events occurring after rainfall mainly appear to the condition $H_1/SWI < 0.2$, which indicates

that the rainwater had infiltrated deeper soil layers when these landslides occurred, and less soil moisture remained in the surface soil.

Concerning the second tank water depth fraction distribution, regardless of the condition they occurred, 90% of DF events, 83% of SL events, and 69% of LL events had a H_2/SWI value in the range of 0.2–0.4. Some instances of LL occurred when H_2/SWI was in a range of 0.4–0.5. These matched the type 3 condition in Fig. 12a, representing the deeper layer's water infiltration. In addition, a small number of all types of landslides happened when the $H_2/SWI < 0.2$. The cases in the left down zone matched type 1 in Fig. 12a, showing that DF, SL, and LL can occur in the early stage of the rain. The right-down cases are the after-rain LL, matching the type 4 (Fig. 12a). This is consistent with our understanding that the rise of the water table may cause LL. However, compared to the H_1/SWI and H_3/SWI distribution, the H_2/SWI distribution is relatively narrow, and there is no significant difference in the H_2/SWI distribution for the three types of landslides.

Concerning the third tank fraction distribution, 78% of DF events occurred when $H_3/SWI < 0.3$, while SL and LL events occurring during rainfall were relatively distributed. However, the types of landslides have H_3/SWI in the order LL > SL > DF. This phenomenon can be explained by the occurrence time. Since SL and DF have shorter occurrence times than LL (as shown in Fig. 4), the water in the soil can disperse quickly and is not replenished continuously by rainfall. The H_3/SWI ratio of the most LL occurring after rainfall was in the range of 0.5–0.9, which indicates that as rainfall duration increases, LL events are likely to be controlled by the third tank water depth fraction.

In general, the H_2/SWI distribution is consistent with the three types of landslides, which suggests that the ratios H_1/SWI and H_3/SWI are the critical factors in the occurrence of landslides. Changes in these ratios can also explain landslide type changes. The ternary diagram shows that when H_2/SWI is in the 0.2–0.4 range, the landslide's predominant type gradually shifts from DF to SL and then to LL along the H_3/SWI axis.
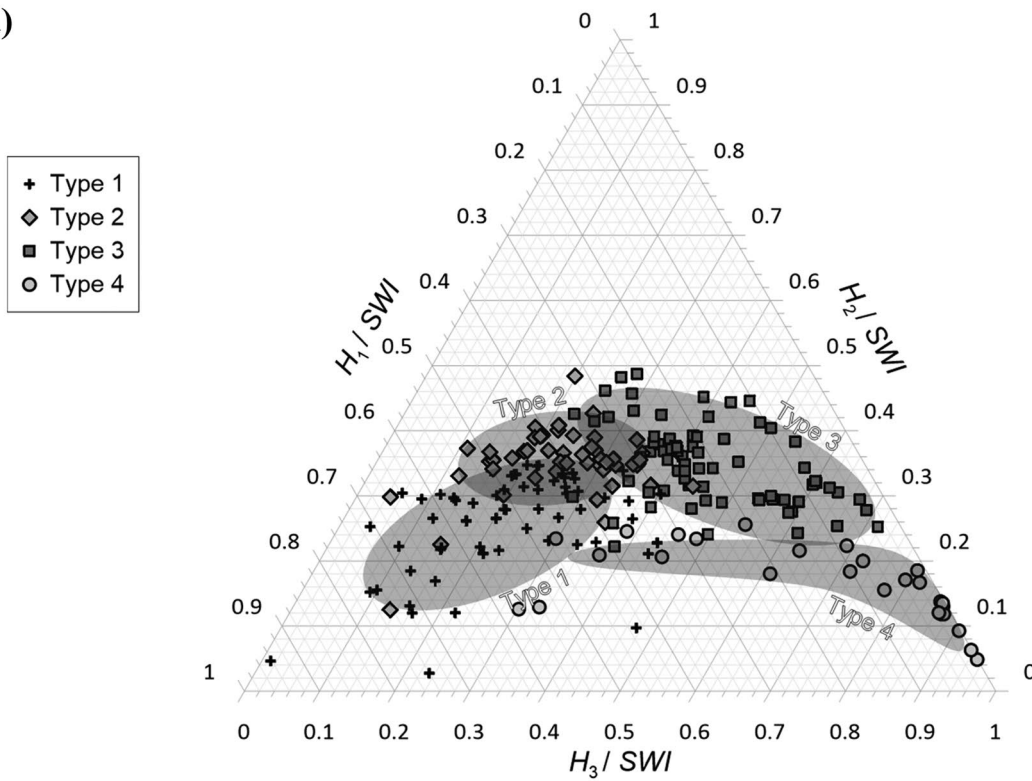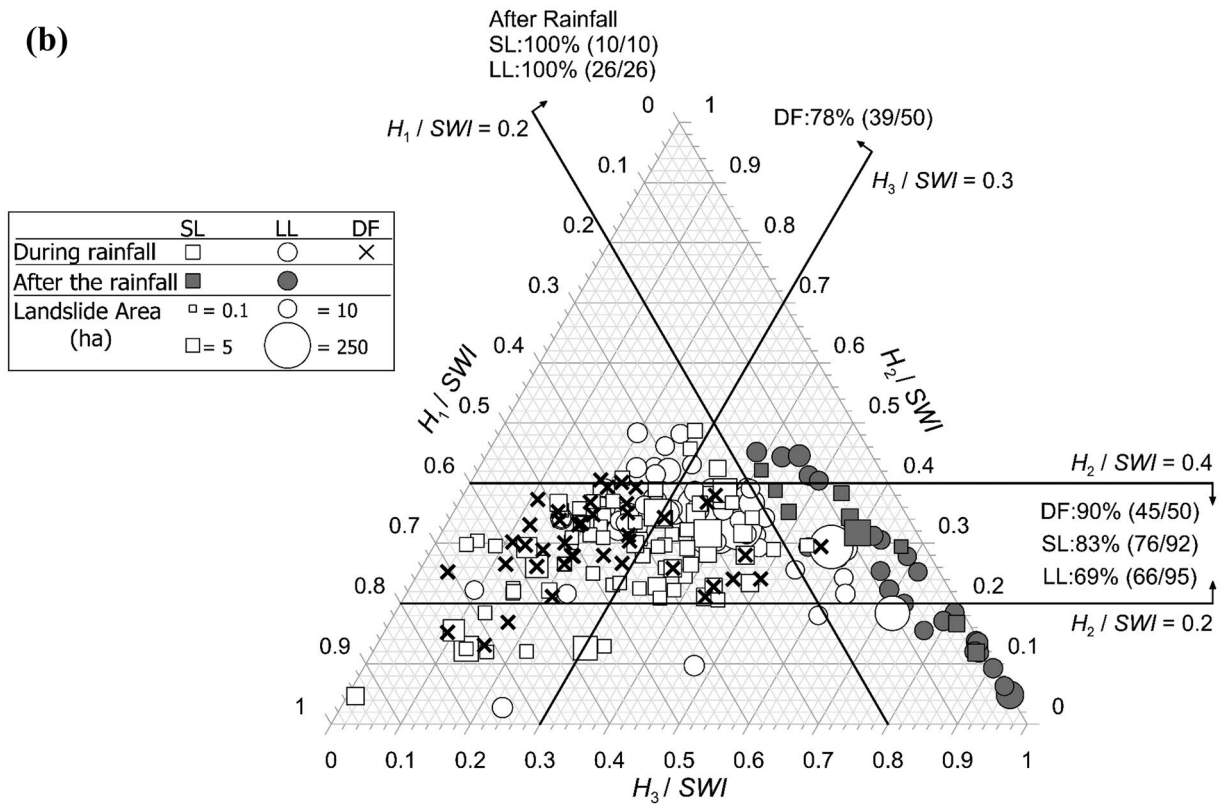
Fig. 12 The ternary diagram of water depth factions in three tanks with landslide occurrences clustering in **a** the water depth variation conditions in each tank (according to the classification in Fig. 11) and **b** the landslide types (DF, SL, LL)

Conclusions

We adopted the soil water index (*SWI*) approach to investigate the characteristics of three types of rainfall-induced landslides, namely debris flows (DF), shallow landslides (SL), and large-scale landslides (LL) in Taiwan. Our results indicate that DF events either occurred during rainfall, mainly when rainfall intensity > 10 mm/h, or within the period from maximum rainfall intensity to 3 h afterward. The positive correlation was found between DF and rainfall intensity. Furthermore, DF had a median *SWI* of 236 mm and a median occurrence time of 21 h, and DF had the highest water depth fraction in the first tank (the most significant H_1/SWI value). This indicates that the occurrence of DF events is connected with the water depth in the first tank. Most DF events occurred in the type 1 situation, where water depths in the three tanks are rising.

SL and LL landslides occurred in a broad rainfall intensity distribution, and some landslides occurred after rainfall stopped. Rainfall intensity alone cannot correlate well with SL and LL occurrence times. Furthermore, accumulated rainfall cannot explain the after-rainfall occurrence of SL and LL well. Because water moisture content strongly influences SL and LL's occurrence time, the *SWI* represents the key factor. The median *SWI* of SL was 206 mm, the median SL landslide occurrence time was 19 h, and SL and LL have similar H_1/SWI and H_2/SWI ratios. Most SL events occurred during type 1 and type 2 situations, which prevail during the initial period of rainfall events or when the rainfall intensity starts to decrease. We found that the *SWI* can better explain the occurrence of landslides controlled by downward seepage after rainfall has diminished or stopped.

In comparison with DF and SL, LL have significantly different characteristics. The first difference is that rainfall intensity is not the chief factor influencing the occurrence of LL events. The median *SWI* of LL was 271 mm, and the median landslide occurrence time was 41 h, which are greater than those of DF and SL. LL occurring after rainfall had the greatest H_3/SWI ratio, which indicates that LL after rainfall are controlled by soil moisture in the deep layer. Most LL events are type 3 and type 4, where rainfall almost stops, and rainwater already infiltrates deeper layers. Consequently, LL mainly occur in the period near the peak H_3 value. We also found that LL after rainfall essentially occurred within an interval of 1.0–1.2 times the rainfall duration. Therefore, the period within $1.2T_R$ can be assumed as the time in which LL events have the potential to occur. The three types of landslides have relatively consistent H_2 distribution in the SWI ternary diagram. H2/*SWI* concentrates in the range of 0.2–0.4, within which the landslide instance clusters shift along the H_3/SWI axis from DF to SL and then to LL. The SWI ternary diagram is an excellent tool to explain how the landslide type shifts along with tank depth ratios.

Author contribution

Conceptualization: Su-Chin Chen and Yi-Jun Liu; data curation: Su-Chin Chen; methodology: Yi-Jun Liu and Yen-Yu Chiu; analysis: Yi-Jun Liu, Yen-Yu Chiu, and Frank T.-C. Tsai; supervision: Su-Chin Chen; writing of the original draft: Yi-Jun Liu; writing including review and editing: Yen-Yu Chiu, Frank T.-C. Tsai, and Su-Chin Chen.

References

Bogaard T, Greco R (2018) Invited perspectives: hydrological perspectives on precipitation intensity-duration thresholds for landslide initiation: proposing hydro-meteorological thresholds. Nat Hazards Earth Syst Sci 18:31–39. https://doi.org/10.5194/nhess-18-31-2018

Brunetti MT, Peruccacci S, Rossi M, Luciani S, Valigi D, Guzzetti F (2010) Rainfall thresholds for the possible occurrence of landslides in Italy. Nat Hazard Earth Sys 10:447–458. https://doi.org/10.5194/nhess-10-447-2010

Caine N (1980) The rainfall intensity–duration control of shallow landslides and debris flows. Geogr Ann 62:23–27. https://doi.org/10.2307/520449

Chen CW, Saito H, Oguchi T (2017) Analyzing rainfall-induced mass movements in Taiwan using the soil water index. Landslides 14:1031–1041. https://doi.org/10.1007/s10346-016-0788-1

Chen SC, Tsai CW, Chen CY, Chen MC (2013) Soil water index applied as a debris flow warning-reference based on a tank model. J Chin Soil Water Conserv 44(2):131–143

Dammeier F, Moore JR, Haslinger F, Loew S (2011) Characterization of alpine rockslides using statistic alanalys is of seismic signals. J Geophys Res Earth Surf 116:F04024. https://doi.org/10.1029/2011JF002037

Dille A, Kervyn F, Mugaruka Bibentyo T, Delvaux D, Ganza GB, Ilombe Mawe G, Kalikone Buzera C, Safari Nakito E, Moeyersons J, Monsieurs E, Nzolang C, Smets B, Kervyn M, Dewitte O (2019) Causes and triggers of deep-seated hillslope instability in the tropics – insights from a 60-year record of Ikoma landslide (DR Congo). Geomorphology 345(106):835. https://doi.org/10.1016/j.geomorph.2019.106835

Gariano SL, Guzzetti F (2016) Landslides in a changing climate. Earth Sci Rev 162:227–252. https://doi.org/10.1016/j.earscirev.2016.08.011

Guzzetti F, Peruccacci S, Rossi M, Stark C (2007) Rainfall thresholds for the initiation of landslides in Central and Southern Europe. Meteorog Atmos Phys 98:239–267. https://doi.org/10.1007/s00703-007-0262-7

Hutchinson JN (1988) General Report: Morphological and geotechnical parameters of landslides in relation to geology and hydrogeology. Proceedings. General Report, Fifth International Symposium on Landslides 1:3–35

Ishihara Y, Kobatake S (1979) Runoff model for flood forecasting. Bulletin of Disaster Prevention Research Institute, Kyoto University 29:27–43. http://hdl.handle.net/2433/124881

Jan CD, Lee MH (2004) A debris-flow rainfall-based warning model. J Chin Soil Water Conserv 35:275–285

Kuo HL, Lin GW, Chen CW, Saito H, Lin CW, Chen H, Chao WA (2018) Evaluating critical rainfall conditions for large-scale landslides by detecting event times from seismic records. Nat Hazards Earth Syst Sci 18(11):2877–2891. https://doi.org/10.5194/nhess-18-2877-2018

Larsen M, Simon A (1993) A rainfall intensity–duration threshold for landslides in a humid-tropical environment. Puerto Rico Geogr Ann 75:13–23. https://doi.org/10.1080/04353676.1993.11880379

Lee MH (2006) The rainfall threshold and analysis of debris flows. Dissertation, National Cheng Kung University, Taiwan, ROC

Lin GW, Kuo HL, Chen CW, Wei LW, Zhang JM (2020) Using a tank model to determine hydro-meteorological thresholds for large-scale landslides in Taiwan. Water 12:253. https://doi.org/10.3390/w12010253

Manconi A, Picozzi M, Coviello C, De Santis F, Elia L (2016) Real-time detection, location, and characterization of rockslides using broadband regional seismic networks. Geophys Res Lett 43:6960–6967. https://doi.org/10.1002/2016GL069572

Michiue M (1985) A method for predicting slope failures on cliff and mountain due to heavy rain. J Nat Disaster Sci 7(1):1–12. https://doi.org/10.1016/0148-9062(87)90777-7

Nash JE (1957) The form of the instantaneous unit hydrography. Int Assoc Sci Hydrology 45(3):114–121

Obeysekera J, Salas JD (2016) Frequency of recurrent extremes under nonstationarity. J Hydrol Eng 21(5):04016005. https://doi.org/10.1061/(ASCE)HE.1943-5584.0001339

Okada K, Makihara Y, Shimpo A, Nagata K, Kunitsugu M, Saito K (2001) Soil Water Index Tenki 47:36–41 (in Japanese)

Osanai N, ShimizuT KK, Kojima S, Noro T (2010) Japanese early-warning for debris flows and slope failures using rainfall indices with radial basis function network. Landslides 7(3):325–338. https://doi.org/10.1007/s10346-010-0229-5

Rosi A, Segoni S, Catani F, Casagli N (2012) Statistical and environmental analyses for the definition of a regional rainfall threshold system for landslide triggering in Tuscany (Italy). J Geogr Sci 22:617–629. https://doi.org/10.1007/s11442-012-0951-0

Safran EB, Anderson SW, Mills-Novoa M, House PK, Ely L (2011) Controls on large landslide distribution and implications for the geomorphic evolution of the southern interior Columbia River basin. Geol Soc Am Bull 123(9–10):1851–1862. https://doi.org/10.1130/B30061.1

Saito H, Nakayama D, Matsuyama H (2010) Relationship between the initiation of a shallow landslide and rainfall intensity–duration thresholds in Japan. Geomorphology 118:167–175. https://doi.org/10.1016/j.geomorph.2009.12.016

Sangelantoni L, Gioia MF (2018) Impact of climate change on landslides frequency: the Esino River basin case study (Central Italy). Nat Hazards 93:849–884. https://doi.org/10.1007/s11069-018-3328-6

Sugawara M (1961) On the analysis of runoff structures about several Japanese rivers. Jap J Geophys 2:1–76

Sugawara M, Ozaki E, Watanabe I, Katsuyama Y (1974) Tank model and its application to Bird Creek, Wollombi Brook, Bikin River, Kitsu River, Sanaga River and Nam Mune. Res Note Natl Res Center Disaster Prev 11:1–64

Suzuki M, Fukushima Y, Takei A, Kobashi S (1979) The critical rainfall for the disasters caused by debris movement. Int J Eros Control Eng 31(3):1–7. https://doi.org/10.11475/sabo1973.31.3_1

Tamura K, Uchida T, Suzuki R, Minori H, Kurihara F (2008) Evaluation of deep seated landslide susceptibility river. Public Works Research Institute, Tech Rep

Tfwala S, Huang CL, Tsou CY, Chen SC (2020) A landslide ternary diagram for geometric form and topographic site in Taiwan. Landslides 18:619–627. https://doi.org/10.1007/s10346-020-01507-2

Wu CY, Tsai CW, Chen SC (2016) Topographic characteristic analysis of landslides in Kaoping River watershed. J Chin Soil Water Conserv 47(3):156–164

Yi-Jun Liu · Yen-Yu Chiu · Su-Chin Chen (✉)
Department of Soil and Water Conservation, National Chung Hsing University, Taichung 40227, Taiwan
Email: scchen@nchu.edu.tw

Frank T.-C. Tsai
Department of Civil and Environmental Engineering, Louisiana State University, Baton Rouge, LA 70803, USA

Su-Chin Chen
Innovation and Development Center of Sustainable Agriculture, National Chung Hsing University, Taichung 40227, Taiwan